
This is an electronic reprint of the original article.
This reprint may differ from the original in pagination and typographic detail.

Jaiswal, Aayush Kumar; Hokkanen, Ari; Khakalo, Sergei; Mäkelä, Tapio; Savolainen, Anniina; Kumar, Vinay

Thermochromic Nanocellulose Films for Temperature-Adaptive Passive Cooling

Published in:
ACS Applied Materials and Interfaces

DOI:
[10.1021/acsami.3c18689](https://doi.org/10.1021/acsami.3c18689)

Published: 27/03/2024

Document Version
Publisher's PDF, also known as Version of record

Published under the following license:
CC BY-NC-ND

Please cite the original version:
Jaiswal, A. K., Hokkanen, A., Khakalo, S., Mäkelä, T., Savolainen, A., & Kumar, V. (2024). Thermochromic Nanocellulose Films for Temperature-Adaptive Passive Cooling. *ACS Applied Materials and Interfaces*, 16(12), 15262-15272. <https://doi.org/10.1021/acsami.3c18689>

This material is protected by copyright and other intellectual property rights, and duplication or sale of all or part of any of the repository collections is not permitted, except that material may be duplicated by you for your research use or educational purposes in electronic or print form. You must obtain permission for any other use. Electronic or print copies may not be offered, whether for sale or otherwise to anyone who is not an authorised user.

Thermochromic Nanocellulose Films for Temperature-Adaptive Passive Cooling

Aayush Kumar Jaiswal,* Ari Hokkanen, Sergei Khakalo, Tapio Mäkelä, Anniina Savolainen, and Vinay Kumar



Cite This: *ACS Appl. Mater. Interfaces* 2024, 16, 15262–15272



Read Online

ACCESS |



Metrics & More



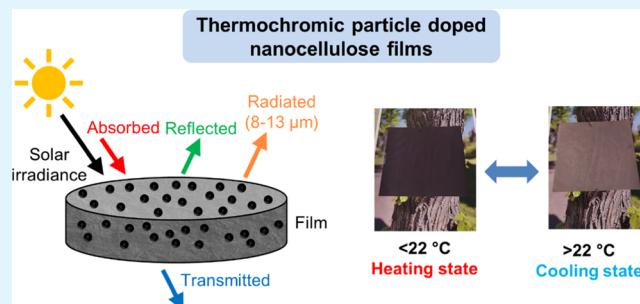
Article Recommendations



Supporting Information

ABSTRACT: Energy efficiency in habitation spaces is a pivotal topic for maintaining energy sufficiency, cutting climate impact, and facilitating economic savings; thus, there is a critical need for solutions aimed at tackling this problem. One viable approach involves complementing active cooling methods with powerless or passive cooling ones. Moreover, considerable scope remains for the development of passive radiative cooling solutions based on sustainable materials. Cellulose, characterized by its abundance, renewability, and biodegradability, emerges as a promising material for this purpose due to its notable radiative cooling potential exploiting the mid-infrared (MIR) atmospheric transmission window (8–13 μm). In this work, we propose the utilization of thermochromic (TC) materials in conjunction with cellulose nanofibrils (CNF) to confer temperature-dependent adaptivity to hybrid CNF films. We employ a concept where high reflection, coupled with MIR emission in the heated state, facilitates cooling, while high visible light absorption in the cold state allows heating, thus enabling adaptive thermal regulation. CNF films were doped with black-to-leuco TC particles, and a thin silver layer was optionally applied to the films. The films exhibited a rapid transition (within 1 s) in their optical properties at ~ 22 $^{\circ}\text{C}$, becoming transparent above the transition temperature. Visible range transmittance of all samples ranged from 60 to 90%, with pronounced absorption in the 8–13 μm range. The cooling potential of the films was measured at 1–4 $^{\circ}\text{C}$ without any Ag layer and ~ 10 $^{\circ}\text{C}$ with a Ag layer. In outdoor field testing, a peak cooling value of 12 $^{\circ}\text{C}$ was achieved during bright sunshine, which is comparable to a commercial solar film. A simulation model was also built based on the experimental results. The concept presented in this study extends beyond applications as standalone films but has applicability also in glass coatings. Overall, this work opens the door for a novel application opportunity for green cellulose-based materials.

KEYWORDS: cellulose, passive cooling, thermochromic, nanocellulose, films and coatings



INTRODUCTION

Energy efficiency in living spaces is a key research topic for maintaining energy sufficiency, lowering climate impact, and enabling cost savings.¹ Heating, ventilation, and air conditioning (HVAC) systems can account for 20–25% of energy consumption in buildings, especially in hot climates where active cooling methods such as fans and air conditioners are heavily used.² The International Energy Agency (IEA) estimated that HVAC systems will account for roughly 50% of global electricity consumption by 2050.² Therefore, there is a pressing need for solutions to help lower energy consumption in living spaces. One such method is to complement active cooling with powerless or passive cooling.

Passive cooling methods include architectural solutions enabling cross ventilation, increasing shaded areas in buildings, using green roofs, etc., and technical solutions such as radiative cooling materials that can be applied to windows and exterior surfaces of buildings.³ Passive radiative cooling is ideally achieved using a combination of high solar rejection and high

infrared (IR) emittance, particularly in the 8–13 μm range, which is the transparency window in the Earth's atmosphere.^{4,5} Nighttime passive cooling is a well-studied phenomenon, but the possibility of daytime subambient passive cooling was reported for the first time in 2013.⁶

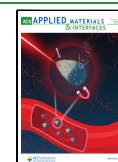
Since then, in the literature, passive daytime radiative cooling structures have been achieved using reflective pigments like TiO_2 , ZnO , ZnS , and BaSO_4 ,^{7–10} IR resonators like SiO_2 and SiC ,^{11–13} all-dielectric Bragg mirrors,¹⁴ and a variety of photonic stacked structures involving materials such as Si, Ag, Al, MgF_2 , SiO_2 , and HfO_2 .^{6,15–18} These developments have also led to the launch of commercial products on the market,

Received: December 13, 2023

Revised: February 27, 2024

Accepted: March 1, 2024

Published: March 14, 2024



for instance, Passive Radiative Cooling Film from 3M, cooling foils from SPACECOOL Inc., and cooling panels from SkyCool Systems.

However, there is still room to develop such passive radiative cooling solutions based on sustainable materials. One promising material for this application is cellulose—an abundant, renewable, and biodegradable material that also offers radiative cooling potential with its high mid-IR range absorbance (8–13 μm).¹⁹ Cellulose is a carbohydrate polymer that is the structural unit of plant fibers but it is also synthesized by certain bacteria and termed as bacterial cellulose.²⁰ Cellulose fibers can be processed through various established chemical, enzymatic, or mechanical processes to obtain cellulose nanomaterials, often termed as nanocellulose.^{21,22} Nanocellulose is classified based on its morphology as either cellulose nanofibrils (CNFs) or cellulose nanocrystals (CNCs).^{23,24}

Cellulose-based passive radiative coolers were first investigated by the Jonsson group at Linköping University. In the first such report, Gamage et al. developed hybrid films with SiO₂ microparticles and CNF which had high thermal emission and low visible light absorption that enabled ca. 3 °C cooling impact.¹² This work was followed by porosity-based modulation of the reflectivity to afford both highly transparent and highly reflective cellulose-based cooling films. The transparent films prepared via self-assembly of carboxymethylated CNF showed a 5 °C cooling impact, and the reflective films prepared via electrospinning of cellulose acetate fibers (and further regeneration into native cellulose) showed a remarkable 15 °C cooling impact.²⁵ Recently, structurally colored CNC-glucose hybrid films were demonstrated as radiative coolers with up to 9 °C cooling impact.²⁶

Other cellulose-based passive cooling reports in the literature include the use of native cellulose–SiO₂ composite films as 24 h radiative coolers with a cooling potential of 6 °C during the day and 8 °C at night.²⁷ In another such work, cellulose acetate films were doped with TiO₂ particles to achieve a peak 10 °C cooling impact in outdoor measurements.²⁸ Lv et al. demonstrated the use of a cellulose membrane inside a crystalline Si solar module assembly to achieve a 2 °C cooling effect which increased the module efficiency.²⁹

As much as cooling needs are important, switching the passive cooling performance to heating is essential for year-round viability in climates with strong seasonal temperature variation, in terms of both thermal comfort and energy savings.^{30,31} Hence, adaptive passive thermal regulation systems are sought after. Dastidar et al. demonstrated so-called Janus cellulose film, which had an adaptive cooling/heating feature triggered by wetting, using a multilayer structure composed of a porous electrospun cellulose fiber layer placed upon a hybrid layer of CNF and carbon nanotubes (CNTs).³² Using the same approach, Fei et al. demonstrated a porous cellulose acetate film with adaptive cooling and heating feature when in dry and wet state, respectively.³³

In this report, we propose the use of thermochromic (TC) materials in combination with CNF to impart temperature-driven adaptivity to the CNF-based cooling films. TC materials change their color, reversibly or irreversibly, in response to temperature variation where the color transition can be from colored to either another color or to colorless.³⁴ In our earlier work, we reported the first nanocellulose–TC particle hybrid films which were black colored at temperatures <31 °C and

turned transparent at higher temperatures to realize all-optical modulation.³⁵ Now, we employ similar films where high reflection coupled with MIR emission under hot temperatures would enable cooling, whereas high visible light absorption in the cold state would allow heat gain, thus enabling adaptive thermal regulation. Additionally, we supplement the concept with thin Ag layer deposition on the films. To our knowledge, there has not been any prior report in the literature where the impact of adding TC materials to nanocellulose films for adaptive passive thermal regulation application has been studied. Hence, our work creates a novel opening for further investigation of nanocellulose–thermochromic hybrid metamaterials.

EXPERIMENTAL SECTION

Materials. CNF suspension was produced via mechanical homogenization of bleached hardwood (Birch) kraft pulp in a grinder (Supermasscolloider MKZA10–15J, Masuko Sangyo Co., Japan). After homogenization, the pulp suspension was fed into a microfluidizer (M-7115–30, Microfluidics) where a total of six passes were made through the microfluidizer at 1800 bar pressure. The first pass utilized chambers of diameters 500 and 200 μm , and the next five passes were through 500 and 100 μm chambers. A translucent viscous gel was obtained after the treatment with a final solid content of 1.7% and pH of 6.4. D-sorbitol with >98% purity (Merck GmbH, Germany) was used as a plasticizer for all CNF films in 20% w/w addition level on dry CNF. D-sorbitol powder was dissolved in deionized water at 50% (w/w) concentration prior to use in formulations.

Leuco dye TC microcapsules (Chromazone Black 22) were purchased from TMC Hallcrest Ltd., United Kingdom, as an aqueous slurry (50% solids content). The TC pigments were black in the cold state, and a leuco transition occurred at a nominal temperature of 22 °C. Chromazone pigments are available in a range of colors and transition temperatures, but in this work, black pigments and 22 °C were chosen to maximize solar gain control and to correspond to the room temperature, respectively. Three different pigment addition levels, viz., 5, 10, and 20% (on dry cellulose mass), were used in this study.

Commercial solar glass and solar films were used as reference materials. Sunergy Gray solar glass with 6 mm thickness and solar control coating on one side was kindly provided by AGC Glass Europe. Two types of solar films were purchased from Biltema Suomi Oy, Finland, with nominal visible range transparency of 15% (product code 39–772) and 5% (product code 39–774), respectively. In this study, the solar films were termed “Solar film 15%” and “Solar film 5%”, respectively. Both films were 60 μm thick.

Methods. Fabrication of Films. Thermoresponsive nanocellulose films were prepared by suspension casting. First, a casting formulation was prepared by mixing the CNF suspension, TC particle suspension, D-Sorbitol solution, and deionized water in the desired ratio to yield a formulation at 1.5% (w/w) solids content. The mixture was stirred at low shear for 30 min to ensure homogeneity. Lastly, the formulation was deaerated using an asymmetric vacuum-aided centrifuge (SpeedMixer DAC 600, Synergy Devices Ltd., United Kingdom) for 5 min at 1400 rpm and 0.9 bar of vacuum.

The casting formulation was applied onto a flat polyethylene terephthalate (PET) film (optimont MF-AS, Bleher Folientechnik GmbH, Germany) using a gap coating knife with a 3 mm gap. The PET film was treated with a corona discharge of 200 W (LabTEC-X, Tantec, Denmark) before film casting to improve surface wetting. The casted film size was 20 × 20 cm². The wet films were dried at 23 °C and 50% relative humidity (RH) for 24 h and then peeled off from the PET substrate to obtain standalone films. The target basis weight of the films was 50 g·m⁻² to enable easy handling. Post preparation, all film samples were stored at 23 °C and 50% RH.

Silver (Ag) layers were deposited on the films via a physical vapor deposition (PVD) technique using a thermal metal evaporation

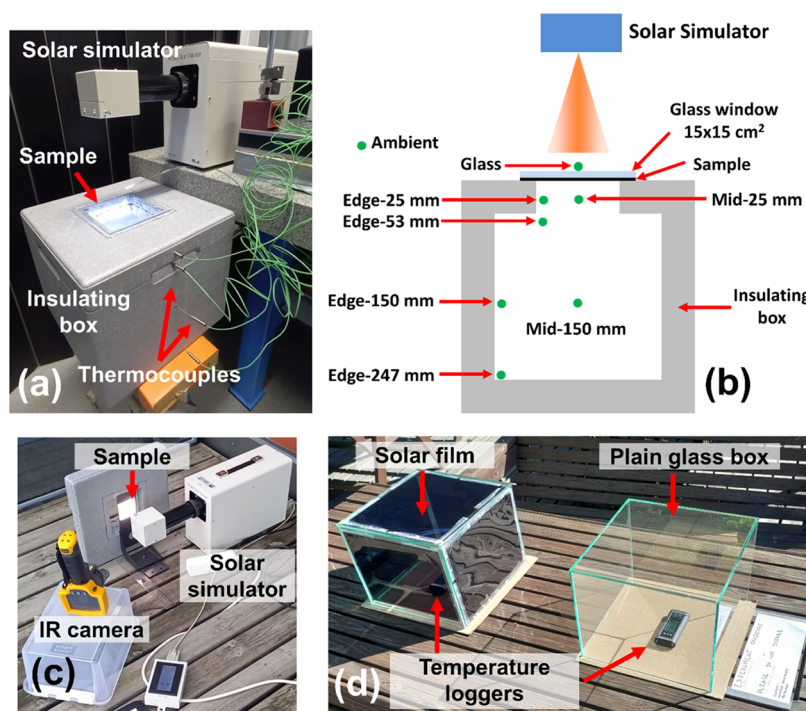


Figure 1. (a) Cooling potential measurement setup using a solar simulator lamp and an insulating box equipped with thermocouples. (b) Schematic of the cooling measurement setup where the positions of the thermocouples are marked as green dots. (c) Outdoor setup for film surface temperature measurement with a solar simulator and an IR camera. (d) Setup for outdoor glass box heating measurements.

apparatus MB200B (MBRAUN, Germany). A $15 \times 15 \text{ cm}^2$ film was placed in the vacuum chamber, and vacuum was pumped down for at least 3 h to achieve a target evaporation vacuum of 1×10^{-6} mbar. Ag pellets (1–3 mm, purity 99.99%, Testbourne Ltd., United Kingdom) and an alumina-coated basket heater (Kurt J. Lesker Company) were used. An evaporation rate of $1\text{--}3 \text{ \AA}\cdot\text{s}^{-1}$ was used, and the film was rotated during the evaporation to achieve a uniform coating. Ag deposition was tested on both the smooth and the rough side of the film (the smoother side being in contact with the PET substrate during preparation), and the layer uniformity was found to be much better for deposition on the smoother side. Therefore, the samples used in the study were prepared by Ag deposition on the smoother side of the film. Mild discoloration was observed in the contact area between the film and Ag coating, probably due to a reaction between the film and the evaporated metal. However, the top surface of the Ag layer was glossy and its electrical conductivity was high.

Characterization of Films. Film thickness was measured using an L&W Micrometer 051 (Lorentzen & Wettre AB, Sweden). Basis weight of the films was calculated by measuring the mass of a film sample of a defined size. Both thickness and basis weight were measured after conditioning the samples at $23 \text{ }^\circ\text{C}$ and 50% RH for at least 24 h. Film density ($\text{g}\cdot\text{cm}^{-3}$) was calculated by dividing the basis weight ($\text{g}\cdot\text{m}^{-2}$) by the film thickness (μm).

Scanning electron microscopy (SEM) analysis of the samples was performed with a field emission scanning electron microscope (FE-SEM) (MERLIN, Carl Zeiss) using a secondary electron detector at an acceleration voltage of 2.0 kV. Prior to imaging, sample surfaces were sputter coated with a thin 3 nm Au–Pd layer using an EM ACE600 device (Leica Microsystems).

Halogen Lamp and Optical Spectrum Analyzer for Transmission Spectrum Measurements. Visible and near-infrared (NIR) transmission loss was measured with a Halogen lamp (HK-2000-HP, Ocean Optics Inc.) and an optical spectrum analyzer (OSA) (AQ-6315A, Ando Electric Ltd.) as described in our earlier work.³⁵ The halogen lamp light was collimated with a multimode optical fiber (105/125 μm core/cladding diameter, Thorlabs Inc.) and a fiber collimator (F230FC-1550, Thorlabs Inc.). A multimode optical fiber 400/425 μm (core/cladding) (Thorlabs Inc.) with the same kind of

fiber collimator collected transmitted light to the optical spectrum analyzer. Transmission loss of TC-doped CNF films was measured in 350–1750 nm wavelength range with 10 nm resolution.

Fourier Transform Infrared Spectroscopy (FTIR). Infrared (IR) absorption spectra of CNF-TC films were analyzed with Fourier transform infrared spectroscopy using a Vector22 FTIR spectrometer (Bruker GmbH, Germany). Thirty scans were made with a resolution of 8 cm^{-1} in absorption mode in 400–8000 cm^{-1} wavenumber range (corresponding wavelength range of 1.25–25 μm). All samples were measured in triplicates.

Scattering, Transmission, and Attenuation Measurements. Scattering, transmission, and attenuation of film samples were analyzed using an integrating sphere (IS200–4, Thorlabs Inc.).³⁵ A red (637 nm) diode laser (S4FC637, Thorlabs Inc.) at 1.6 mW power was coupled to a single-mode fiber (9/125 μm core/cladding diameter) and collimated through the integrating sphere with a fiber lens (F230FC-1550, Thorlabs Inc.). Sample film was placed on an input port during transmission and forward scattering measurements. Correspondingly, the sample film was put on an output port in backward scattering measurements. Attenuation was calculated from the other three measured values (forward scattering, backward scattering, and transmission). The light signal was measured with an S120C photodiode sensor and a PM101 power meter interface (Thorlabs Inc.), and the measured signal from the power meter interface was collected with LabVIEW software. The measurements were performed at room temperature.

Indoor Cooling Potential Measurements with Solar Simulator. A solar simulator (PEC-L01, Peccel Technologies Inc., Japan) was used to measure the cooling potential of the samples. The solar simulator was equipped with a xenon lamp having $100 \text{ mW}\cdot\text{cm}^{-2}$ irradiance that corresponds to the natural solar irradiance at 8–10 cm distance from the lamp. The solar simulator irradiated an insulating graphite polystyrene (Neopor, BASF, Germany) box of outer dimensions $35 \times 35 \times 30 \text{ cm}^3$. The wall thickness of the box was 10 cm, and the thermal conductivity of the box material was $0.032 \text{ W}\cdot\text{m}^{-1}\cdot\text{K}^{-1}$. A $13 \times 13 \text{ cm}^2$ hole was cut into the top of the box, which served as a window for holding samples. A clear $15 \times 15 \text{ cm}^2$ glass plate with 3 mm thickness was used as the base window material in all

measurements, and film samples were placed under the glass piece. Eight K-type stainless steel thermocouples (MA-ISK-S15-100-P1-2.0-C2-T, Labfacility Ltd., United Kingdom) were used for temperature measurements at different locations which were connected to two NI9211 interfaces (National Instruments) and LabVIEW software for data logging. The measurement setup is shown in Figure 1a,b.

Thermographic Surface Temperature Measurements. The surface temperature of film samples was measured during solar simulator exposure using an IR thermal imager (Ti32, Fluke Inc.). A solar simulator lamp was placed at a 9 cm distance from the sample to simulate film temperature change with 1× Sun intensity (100 mW·cm⁻²). For these experiments, both front and back surface temperatures were intended to be analyzed, and this was not possible with a closed box. Therefore, a vertical window setup was prepared, as shown in Figure 1c. Surface temperature measurements were performed at both 24 °C (indoor) and 9.5 °C (outdoor).

Outdoor Glass Box Measurements. Outdoor cooling experiments were performed using two identical glass boxes of 25 × 25 × 20 cm³ dimensions, constructed of 4 mm thick clear glass (Figure 1d). The glass boxes were open from the bottom to allow for the placement of temperature sensors inside the boxes. Once the sensors were positioned, the box was closed with an insulating carton board and placed on a table located under direct sunlight on a clear weather day. Temperature inside both boxes and the ambient temperature were measured with three identical temperature loggers (EL-SIE 2+, Lascar Electronics, United Kingdom). The first box was covered with a cooling film sample, and the second box was a pure glass reference. The measurements were performed in Otaniemi, Espoo, Finland (60.18° N, 24.82° E). Solar irradiance data for the particular measurement day were obtained from the Kumpula observation station of the Finnish Meteorological Institute.

Finite Element Modeling. Finite element (FE) software COMSOL Multiphysics (heat transfer with surface-to-surface radiation) was used for modeling the thermal performance of the nanocellulose films. The FE models were developed following four main steps: (i) to define and create the geometry sequence for the model component, (ii) to specify material properties, (iii) to specify the analysis type, boundary, and initial conditions, and (iv) to mesh the geometric entities. In the heat transfer module, a quadratic Lagrange discretization was used. In the surface-to-surface radiation module, the radiative properties were selected to be wavelength-dependent. Ray shooting was used as a radiation method with linear discretization for the surface radiosity. The solar simulator was modeled via (point) external radiation source as discussed in the Supporting Information (finite element model of solar simulator). An insulating graphite polystyrene box was modeled as a solid thermally conductive material with diffuse surfaces. Air was modeled as a fully transparent thermally conductive fluid (without convection). Glass was modeled as a solid thermal conductive material with semitransparent surfaces. The CNF-TC and Ag layers of the films were modeled as semitransparent thermal conductive solid shells. Basic material properties, such as thermal conductivity (*k*), heat capacity at constant pressure (*C_p*), and density (*ρ*), as well as surface (radiative) properties, namely, emissivity (*ε*), reflectivity (*r*), and transmissivity (*τ*), are presented in Tables 1 and 2, respectively. The values were taken from either a COMSOL Multiphysics material library or web sources. The FE models were developed by utilizing the

Table 1. Basic Properties of Materials Used in the Solar Simulations

material	<i>k</i> , [W/(m·K)]	<i>C_p</i> , [J/(kg·K)]	<i>ρ</i> , [kg/m ³]
polystyrene	0.032	1300	30
glass	1	800	2500
CNF-TC20 film	1	1400	1300
silver	429	235	10,500
wood	0.18	1900	670

actual dimensions of the experimental setups, which are specified in descriptions of the indoor and outdoor cooling experimental setups.

RESULTS AND DISCUSSION

Thermochromic Functional Films. In this work, stand-alone films were prepared using CNF and TC particles with a transition temperature of 22 °C. The films were prepared using a water-based casting method where the concentration of TC particles in the films was varied between 0, 5, 10, and 20% (on dry cellulose mass). Film samples were also coated with thin (<200 nm) reflective silver layers. The films were then employed as thermoresponsive materials to enable adaptive space cooling under direct solar irradiance. Sample description and basic physical properties are listed in Table 3. Basic properties of the CNF used in the study are reported in Table S1 in the Supporting Information.

Figure 2a shows a comprehensive collage of digital photographs of the film samples in both warm (24 °C) and cool (6 °C) environments. The image of the CNF film is not shown in the cold environment because there is no adaptive element in the CNF film, and a commercial solar film with 15% transmittance is shown instead. Naturally, the color tone of the film became darker as the concentration of the TC particles in the film increased. Moreover, the optical transparency of the CNF-TC films also decreased with increasing TC concentration. The pure CNF film was highly transparent. In a cool environment, the thermoresponsive effect imparted by the TC particles was clearly observed visually as the films turned dark. It is interesting to note that the transparency of the films can be modulated to be suitable for various applications by varying the TC concentration. For instance, the CNF-TC20 film can be utilized in areas of high solar insolation, such as south-facing terrace roofs, where cooling is desired over transparency, whereas the CNF-TC5 film can be employed in areas where direct sunlight falls only for a short period during the day.

Investigation of the samples with SEM revealed the spherical nature of the TC particles, which are in the form of microcapsules. The film surfaces seemed to contain clusters of TC particles, where some particles/clusters were fully embedded and some were partially embedded in the nanofibrillar network. Regardless, no visible “dusting” of particles from the films was observed even when rubbing the film surface with force. This indicated that even though some TC particles were visible on the film surface, they were firmly held by the nanofibrillar network via full or partial coverage (Figure S3 in the Supporting Information). Covalent or ionic interactions are not expected. Similar observations of TC particle encapsulation into the CNF network in a “spider web”-like manner have been reported in our previous work using a different TC material.³⁵

Optical Properties and Indoor Cooling Measurements. The transmission spectra of visible and near-infrared (NIR) light through CNF films devoid of metal coatings were assessed using a halogen lamp and optical spectrum analyzer (OSA), as shown in Figure 3a. The transmission loss exhibited an increase corresponding to the increase in the concentration of TC particles, while it demonstrated an overall decrease across the wavelength range of 350–1750 nm. Subsequently, the same films were subjected to FTIR analysis, as depicted in Figure 3b, where atmospheric transmission is plotted as a background. The atmospheric transmission spectrum was generated using the ATRAN model, courtesy of Gemini Observatory.³⁶ All CNF samples exhibited pronounced

Table 2. Surface (Radiative) Properties of Materials Used in the Solar Simulations

material	emissivity (ϵ)		reflectivity (r)		transmissivity (τ)	
	$\lambda < 2.5$ [μm]	$\lambda \geq 2.5$ [μm]	$\lambda < 2.5$ [μm]	$\lambda \geq 2.5$ [μm]	$\lambda < 2.5$ [μm]	$\lambda \geq 2.5$ [μm]
polystyrene	0.95	0.95	0.05	0.05	0	0
air	0	0	0	0	1	1
glass	0.04	0.84	0.08	0.08	0.88	0.08
CNF-TC20 film	0.5	0.8	0.1	0.05	0.4	0.15
silver	0.03	0.4	0.94	0.57	0.03	0.03
wood	0.9	0.9	0.1	0.1	0	0

Table 3. Description of the Prepared Films and Physical Properties

sample code	TC addition (% on CNF)	film thickness (μm)	film density ($\text{g}\cdot\text{cm}^{-3}$)
CNF	0	47 ± 2	1.40 ± 0.07
CNF-TC5	5	40 ± 3	1.23 ± 0.10
CNF-TC10	10	44 ± 2	1.23 ± 0.08
CNF-TC20	20	1.30 ± 0.05	

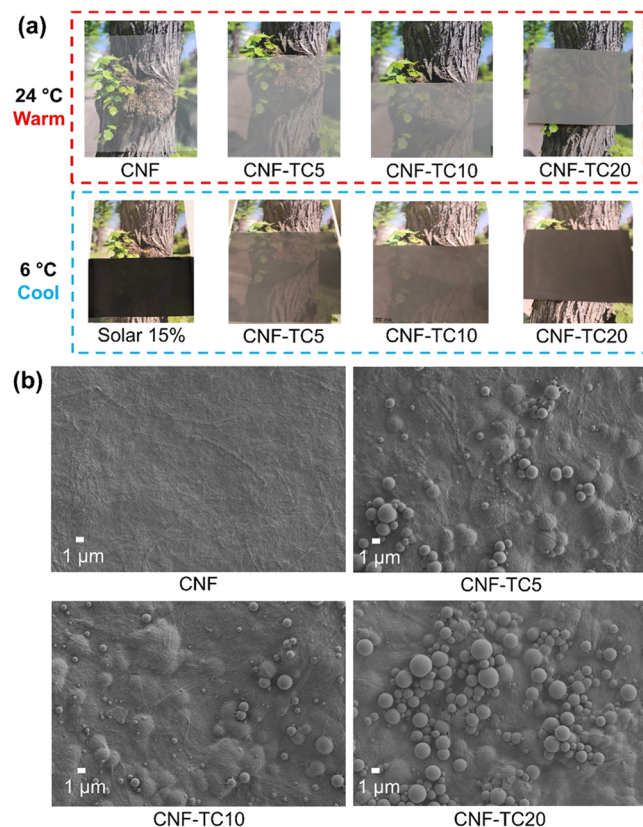


Figure 2. (a) Digital photographs of neat and TC-doped CNF films in warm (24 °C) and TC-doped CNF films in cool (6 °C) environments placed on a printed background image of a tree trunk. A photograph of a commercial solar film (15% nominal transmittance) is added as a reference and shown instead of the CNF film in a cool environment since the CNF film lacks any adaptivity. (b) SEM micrographs of the surface of neat and TC-doped CNF films at 3000 \times magnification.

absorption within the wavelength range 8–12 μm , indicating substantial thermal radiation characteristics in the atmospheric transmission window (8–13 μm), thereby signifying the radiative cooling potential of CNF-based films. This finding is in line with earlier reports in the literature on cellulose-based

films.^{10,12,25} The absorption behavior exhibited a similar dependence on TC concentration and wavelength, as observed in the visible and NIR regions, particularly in the <2.5 μm region.

Transmission, wide-angle forward scattering (haze), backward scattering, and attenuation characteristics of neat and doped CNF films in the absence of metal coatings were evaluated using an integrating sphere and a 637 nm red laser diode. The results are illustrated in Figure 4a, where it can be noted that both transmission and haze exhibited a simultaneous decrease from ~ 90 to $\sim 60\%$ as the TC particle concentration increased. Moreover, almost all of the transmitted light was scattered at wide angles. This occurred due to the relatively coarse size of the CNF material used to fabricate the films. Similar findings have been reported in the literature, where changing the size of the nanocellulose component modulated the haze value. The smaller the nanocellulose component, the lower the haze value obtained.^{35,37} The backward scattering varied between 11–17% and attenuation increased from 0 to 26% when TC doping varied from 0 to 20%.

Indoor cooling potential measurements were performed using a thermocouple-fitted insulated box that was irradiated with a solar simulator lamp (Figure 1a,b). A window was cut into the top of the box to allow light to enter and induce heating, which was measured at various locations in the form of temperature increase. During this experiment, cellulosic film samples were compared with clear glass, commercial solar films, and commercial solar glass in terms of their cooling performance.

A clear 3 mm glass plate was always placed on top of the sample to simulate a practical application, where a cooling film is applied to a window. The glass plate also ensured that the sample film remained flat. Temperature signals of all eight thermocouple sensors were collected (see Figure 1b for sensor layout), and the data from the middle of the box (Mid-150 mm) are shown in Figure 4b,c and from the several other positions in Figure S5 in the Supporting Information. In further discussion, the temperature inside the box is represented as $T_{\text{in,mid}}$ and the ambient temperature has been denoted as T_{amb} .

The Mid-150 mm position is analogous to studying the heating of an object located in a room slightly further from the window, which is under direct solar irradiation. At this position, the plain glass reference, expectedly, showed the highest temperature rise of 10 °C after 700 s lamp exposure. As illustrated in Figure 4b, $T_{\text{in,mid}} - T_{\text{amb}}$ showed a downward trend for CNF-TC films as a function of increasing TC concentration. For instance, a neat CNF film showed a ca. 9 °C temperature rise at 700 s, whereas CNF-TC20 showed a 6 °C rise during the same period. In comparison, the commercial solar glass and solar film exhibited a temperature gain of 5 and

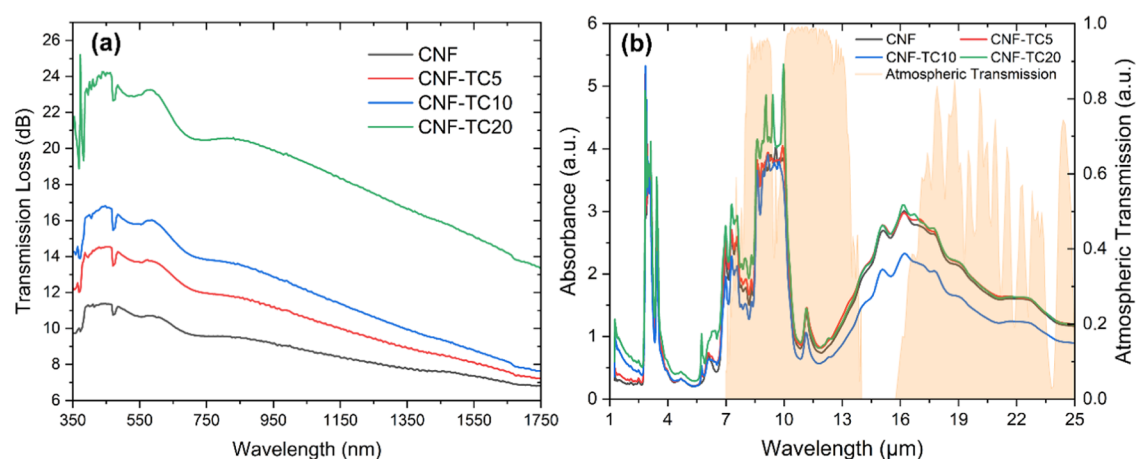


Figure 3. (a) Visible and NIR transmission loss and (b) IR absorption spectrum for CNF films with 0–20% TC doping. The orange shaded background in panel (b) depicts the Earth's atmospheric transmission window.

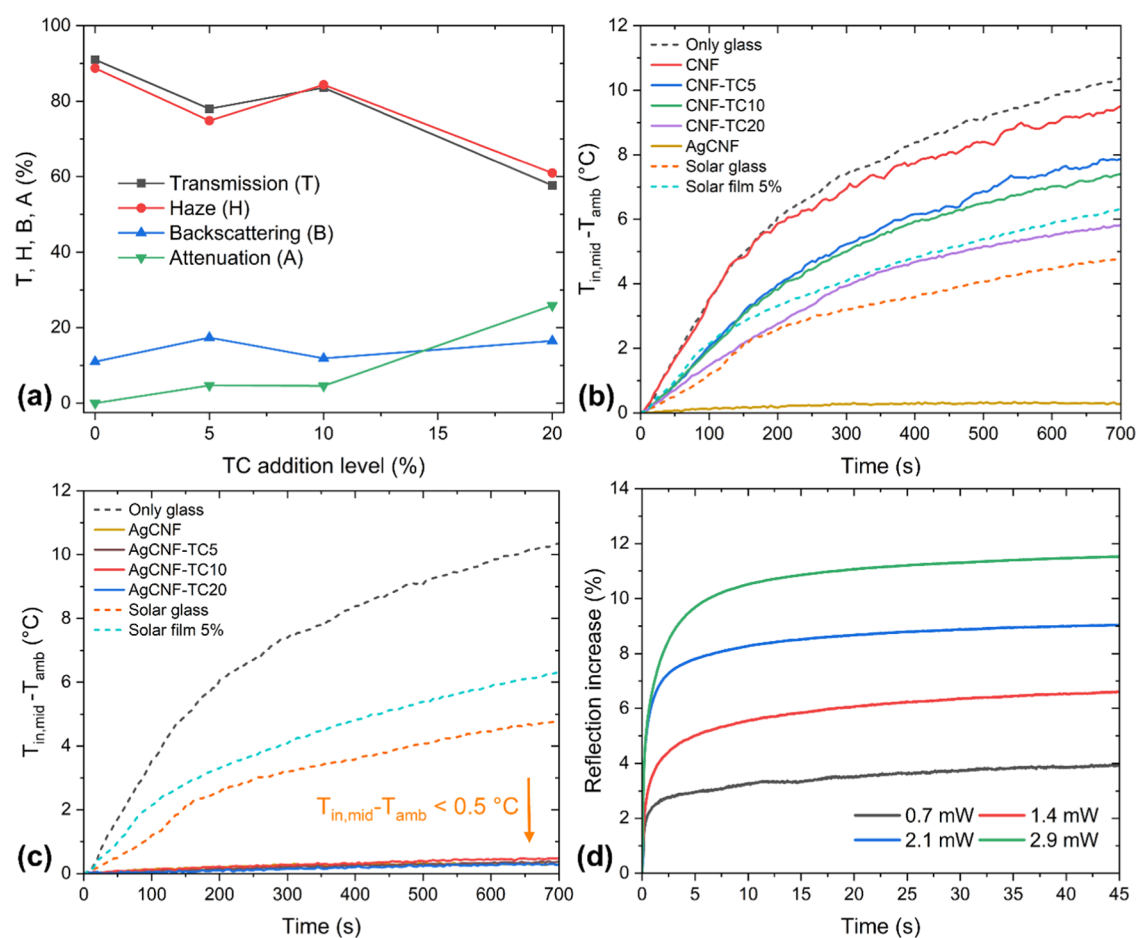


Figure 4. (a) Transmission, haze, backscattering, and attenuation for CNF film samples as a function of the TC concentration (at 637 nm). (b) $T_{in,mid}$ evolution relative to T_{amb} inside the insulated box upon solar simulator irradiance for film samples compared to a clear glass window, a commercial solar glass, and a commercial solar film. The $T_{in,mid}$ data were collected from the Mid-150 mm position, i.e., middle of the insulating box, 150 mm below the sample, and directly under the irradiance from the solar simulator lamp. T_{amb} was collected with a thermocouple placed outside the box. (c) Similar measurements as shown in panel (b) but with metalized CNF films. (d) Reflection increase for the AgCNF-TC20 sample upon optical heating with a 637 nm laser at different power levels.

6 °C, respectively. This concludes that even without metal coating, the CNF-TC films were able to provide a cooling effect similar to that of the commercial references.

The metalized film samples, i.e., AgCNF-TC films showed almost no temperature increase, with $T_{in,mid} - T_{amb} < 0.5$ °C,

independent of TC concentration, as shown in Figure 4c. This implies that a 200 nm thick Ag layer renders the film too opaque. Nevertheless, the thermochromic functionality of the film remains intact (Figure 4d). Such a film could be utilized in applications where cooling performance is desired but

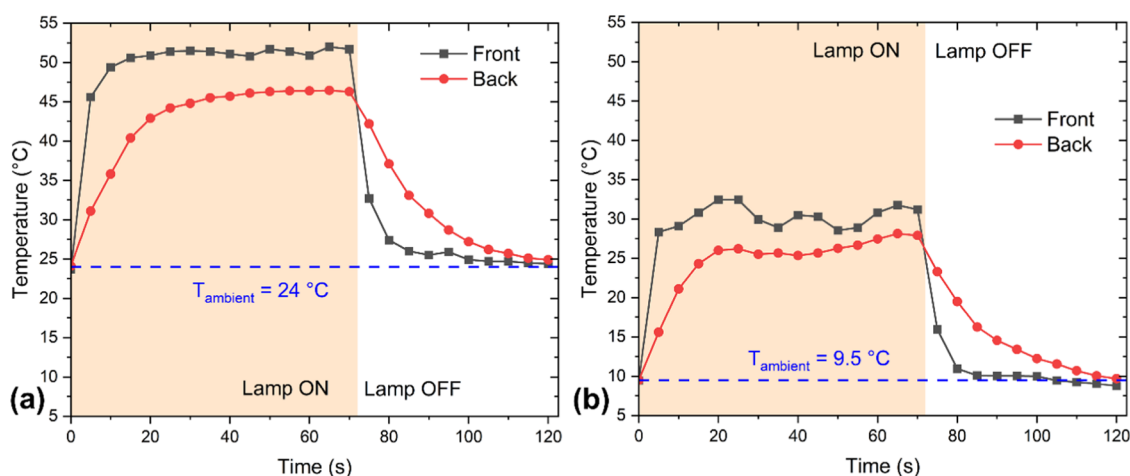


Figure 5. Front (non-Ag side) and back (Ag side) surface temperatures of the AgCNF-TC20 sample films under solar simulator exposure (a) in the laboratory at 24 °C and (b) outdoors at 9.5 °C. The orange shaded part indicates the heating period when the lamp was ON (up to 72 s), and the white portion indicates the film cooling period (lamp OFF).

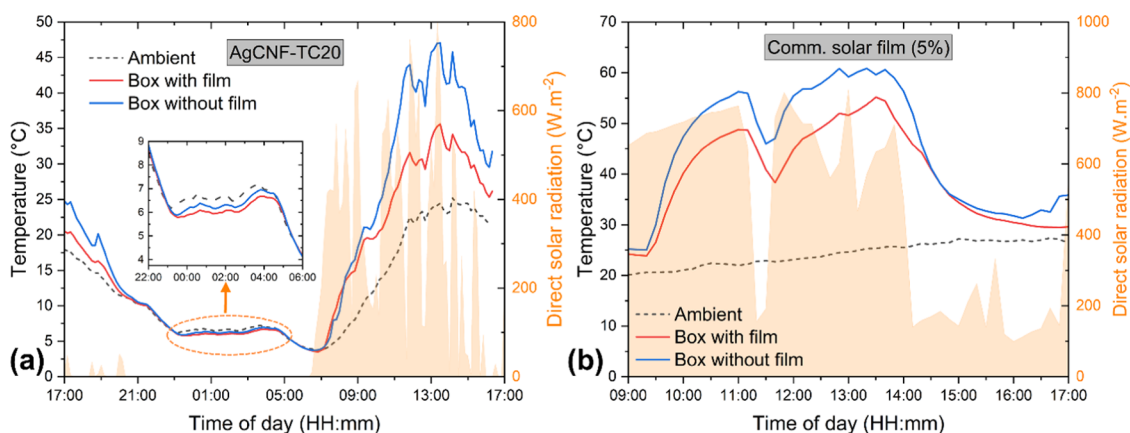


Figure 6. Outdoor glass box measurements: (a) performed overnight between 17:00 and 16:00, 5–6th September 2022 and (b) commercial solar film 5% performed between 09:00 and 17:00 on 5th August 2022. The solar radiation data for the corresponding duration are plotted in the background in orange color.

transparency is not required, for instance, in roofs.¹⁵ If needed, the transparency of the films can be increased by either decreasing the Ag layer thickness or applying a patterned Ag layer instead of a continuous one. However, lowering the thickness of the Ag layer to increase the transparency has one practical pitfall. The roughness of CNF films can be in the order of 100 nm and hence, depositing thinner coatings is challenging without avoiding the creation of pinholes in the metal layer.^{38,39} Therefore, patterning of the Ag coating during deposition is a more attractive way to increase film transparency, which could be performed in a facile manner via masking.⁴⁰ In this work, we did not perform patterning of the Ag layer, but we made theoretical estimates for tuning the cooling performance with Ag layers with a defined open (nonmetalized) area (data shown in Figure S6 in the Supporting Information). The computed estimates showed that even with a 50% open area in the Ag layer, the cooling performance could still be similar to the commercial solar glass reference. Such CNF-TC films with patterned coatings hold potential in automobile applications, for instance in sunroofs to lower the energy demand of the HVAC system.⁴¹

In another experiment, the difference between the front and back sides of the sample films was measured via IR

thermography. The surface temperature of the AgCNF-TC20 film was analyzed with an IR camera during solar simulator exposure at two different ambient temperatures—in the laboratory at 24 °C (Figure 5a) and outdoors at 9.5 °C (Figure 5b). The uncoated surface of the film faced the light exposure and was termed as the front side, and the Ag-coated side was termed as the back side. A patch of high emissivity tape (Scotch Super 33+, 3M; emissivity ~0.95) was applied on the back side (Ag side) to allow thermographic measurements since Ag has too low emissivity (see Figure S7 in the Supporting Information).

Figure 5 illustrates that the film surface temperature, on both front and back surfaces, increased rapidly during light exposure and then plateaued. Film surface temperatures plateaued quickly, within 10 s on the front surface and 20 s on the back surface. The temperature difference between the front and back sides of the films was ca. 5 °C, both in laboratory and outdoor conditions. When the solar lamp was turned OFF, surface temperatures dropped to the ambient temperature in 10 s on the front surface and 40 s on the back surface. The lower rate of heating/cooling on the back surface can be attributed to the thickness (thus extra mass) of the high emissivity tape that was used to thermographically measure the

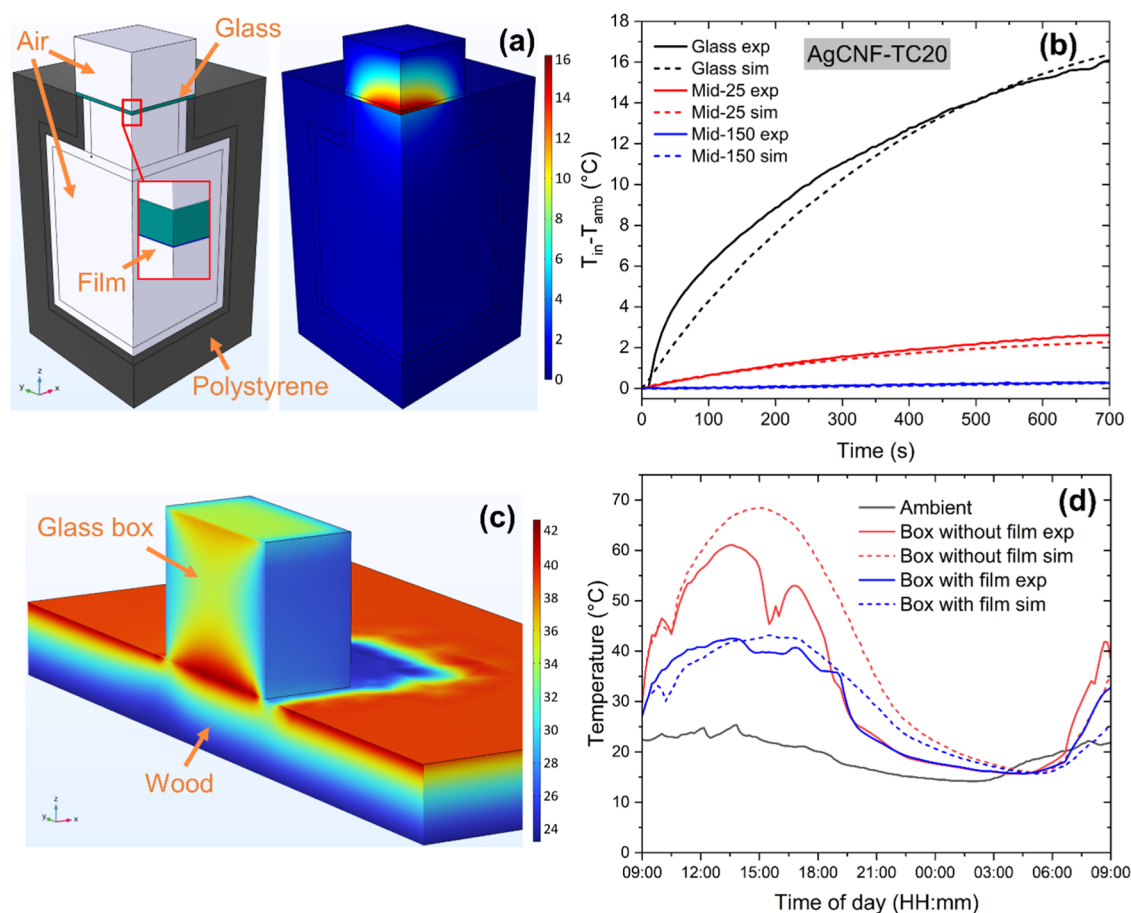


Figure 7. (a) Simulation setup for indoor cooling measurements showing the geometry (insulating box split in a quarter), materials, and the distribution of the temperature field after 700 s of irradiation for the AgCNF-TC20 film sample. The portion inside the red box is enlarged to show the placement of the film sample under the glass plate. (b) Simulated (sim) and experimental (exp) T_{in} evolution relative to T_{amb} at the Glass, Mid-25 mm, and Mid-150 mm positions. (c) Simulation setup for outdoor glass box measurements showing the geometry (glass box sliced from the middle) and the distribution of temperature field at 14:00 for the AgCNF-TC20 film (with 50 nm Ag). (d) Simulated and measured temperatures inside glass boxes placed outdoors, without or covered with the AgCNF-TC20 film between 9:00 and 9:00, 21st–22nd July 2022.

film surface temperature. Slight noise in data was observed during outdoor measurements due to wind effects in the sample surroundings.

Adaptivity with Thermochromic Transition. TC transition-induced adaptivity of films was studied using the AgCNF-TC20 sample via optical spot heating, where the increase in light reflection resulting from the thermochromic transition in the film was examined. This measurement was performed by optically heating the film sample using a red 637 nm diode laser in combination with an integrating sphere, using a method reported in our earlier work.³⁵

Doping of TC particles in CNF films caused an increase in light attenuation (Figure 4a), and this was embodied by light absorption, which led to temperature elevation in the CNF film. The increase in film temperature (above the transition temperature) induced a colored to leuco TC transition, causing the film bulk to turn more transparent. This allowed the Ag layer to be exposed to the irradiation and hence, film reflection to increase. As shown in Figure 4d, the increase in reflection occurred rapidly, within 1 s, and gradually saturated after about 10 s of irradiation. Higher laser power led to a higher change in reflection since the optical heating became stronger. The maximum measured increment in reflection was approximately 12% for the AgCNF-TC20 sample, at a laser

power of 2.9 mW. Hence, the thermoresponsive reflection change in the films could be quantified using this method.

Outdoor Cooling Measurements. Outdoor cooling measurements were performed using a setup consisting of two glass boxes and temperature loggers, as shown in Figure 1d. Ambient temperature was measured with a temperature logger placed outside the glass boxes in a spot shaded from direct sunlight and wind.

Figure 6a illustrates the temperatures inside a glass box fully covered with the AgCNF-TC20 film and an identical glass box with no film in comparison to the ambient temperature. The measurements were started at 17:00 when the sunlight was receding, and this was characterized by the initial temperature drop. It was interesting to note that the temperature inside both the boxes dropped to subambient level at nighttime (shown in the inset), most probably due to the MIR emission properties of both glass and cellulose.^{10,25,42} Post sunrise, the temperatures increased, and the maximum temperatures were recorded in the afternoon under bright sunshine. The uncovered glass box showed the highest temperature of 47 °C, whereas the box with the AgCNF-TC20 film had an ~12 °C lower peak value at the same time when the corresponding ambient air temperature was 24 °C. During the direct solar irradiation period, i.e., 8:00–16:00, the mean temperature

difference was 7.0 ± 3.9 °C between the boxes without and with films.

Figure 6b shows the results from a similar outdoor test where one glass box was covered with a commercial solar film (5% transmittance), and the other box was uncovered. This test was performed only during the daytime (9:00–17:00). A maximum temperature difference of 11 °C between the box with and without films was observed in this test with the mean temperature difference being 5.1 ± 3.2 °C.

Naturally, such outdoor measurement results are specific to a particular date, local weather conditions, and geographical location. Therefore, exact cooling potential values should not be derived from such measurements but from those performed in the laboratory under controlled conditions. Nonetheless, such outdoor measurements are valuable for concept demonstration purposes.

Cooling Performance Modeling. The indoor and outdoor cooling experiments were replicated using finite element (FE) analysis of the heat transfer phenomenon, assuming that thermal conduction and thermal radiation are the main heat transfer mechanisms. Irradiation with a solar simulator lamp was modeled via a point external radiation source as described in the Supporting Information (finite element model of solar simulator). In the AgCNF-TC20 film model, the thicknesses of the Ag and CNF-TC20 layers were set to 200 nm and 42 μm , respectively. The irradiation duration, i.e., simulation step time, was set to 700 s, as in the experimental studies. All parts were modeled as thermal conductive solids except for air which was modeled as thermal conductive fluid. The outer surfaces were subject to a convective heat flux boundary condition with a heat transfer coefficient of $6 \text{ W}\cdot\text{m}^{-2}\cdot\text{K}^{-1}$. Experimentally measured ambient temperature was used as the external temperature in the model.

The simulation setup for modeling indoor cooling potential and the distribution of the temperature field for the AgCNF-TC20 film sample after 700 s of irradiation is shown in Figure 7a (left). The distribution of the temperature field for the AgCNF-TC20 film sample after 700 s of irradiation is shown in Figure 7a (right). For the AgCNF-TC20 film, the surface radiative properties were defined by fitting the simulated temperature data to the experimentally measured data at the Glass, Mid-25 mm, and Mid-150 mm positions. Both the experimental and simulated data are plotted in Figure 7b.

The simulation setup for modeling the outdoor cooling potential is shown in Figure 7c along with an example of the distribution of the temperature field. To simulate the solar irradiation an “external radiation source” was included in the model where the solar position corresponded to the geographical location of the actual outdoor measurements, i.e., Otaniemi, Espoo, Finland (60.18° N, 24.82° E). The incident heat flux was computed for the local solar irradiance data from 21st to 22nd July 2022 between 09:00 and 09:00. The simulations were performed for the glass box with no film and for the glass box fully covered with the AgCNF-TC20 film with a 200 nm Ag layer. The experimental measurements at the aforementioned date were performed with the AgCNF-TC20 film with a 50 nm Ag layer. To reflect this, additional simulations were performed by setting the Ag layer transmissivity value to 0.48.

Figure 7d compares the simulated and measured temperatures inside the glass box. For the box without film, between 9:00 and 11:00, the simulated results very accurately follow the

measured ones, while after 11:00, the simulated results start to deviate, giving a 7.4 °C difference between the peak values. The differences can be explained by the FE model limitations, namely, neglecting thermal convection effects, which, in the case of the uncovered glass box, might be significant. Moreover, the FE model does not take into account hyperlocal weather conditions such as clouds, which can cause large temperature differences. The effect of clouds can be observed between 14:00 and 16:30 in Figure 7d where the experimental curve for the box without film shows a dip. Another factor contributing to the difference between the experimental and the simulated curves is the decreased accuracy of the diode-type temperature sensor at temperatures >55 °C due to photothermal heating of the sensor. Nevertheless, the overall cooling behavior is qualitatively quite accurately captured.

For the glass box fully covered with the AgCNF-TC20 film with a 50 nm Ag layer, between 9:00 and 19:00, the simulated results quite accurately captured the temperature evolution with only a 0.6 °C difference between the peak values. After 19:00, a bit lower cooling rate was observed for the simulated temperature than for the experimental data. Concludingly, the simulation model developed herein is successful in predicting the cooling potential of the developed films. The model can be useful in estimating the cooling potential of such cellulose-based films in different geographical locations with varying amounts of solar radiation and ambient conditions. The model can also be extended to energy savings simulations in future work.

CONCLUSIONS

This work explored the application of sustainable cellulose-based films in thermal regulation for the built environment. CNF films doped with black-to-leuco TC particles were prepared for this purpose. The TC doping levels in the films were 5, 10, and 20% on dry CNF mass. A thin silver layer was also applied to one surface of the film by using vapor deposition. The prepared films were flexible and translucent with a black tint that grew darker as the TC doping in the films was increased. The thermochromic films switched their optical properties rapidly at ca. 22 °C (within 1 s), turning transparent above the transition temperature.

Visible range transmittance of all samples was 60–90%, and all samples exhibited pronounced absorption in the 8–12 μm range corresponding to the atmospheric transmission window. The cooling potential of the films was measured both indoors and outdoors. Indoors, a cooling potential of 1–4 °C was measured with CNF-TC film samples and 10 °C with AgCNF-TC films. Outdoors, a peak cooling value of 12 °C during bright sunshine was measured, which was on par with a commercial solar film. A simulation model was also built based on the experimental results. Temperature-dependent change in film reflectivity was measured using optical heating, where a maximum of 12% reflectivity change (CNF-TC20) was observed as the film heated above 22 °C.

The concept presented in this study is not limited to applications as standalone films but has the potential to be applied as thin glass coatings. Future work on the topic could focus on the coating aspects and on optimizing the reflective coating on the films, for instance, in terms of metal selection, thickness, and patterning of the coating to allow higher transparency. Elaborate durability testing of such films could also be performed, for instance, under prolonged ultraviolet (UV) irradiation and changing humidity. Overall, this work

opens the door for a novel application opportunity for green cellulose-based films.

■ ASSOCIATED CONTENT

SI Supporting Information

The Supporting Information is available free of charge at <https://pubs.acs.org/doi/10.1021/acsami.3c18689>.

Particle size distribution of the TC particles; rheological behavior of film formulations; SEM images of films; supplementary cooling potential measurements; emissivity measurements; and FEM model calibration (PDF) Showing the thermoresponsive nature of the AgCNF-TC20 film in a cold-hot-cold cycle (AVI)

■ AUTHOR INFORMATION

Corresponding Author

Aayush Kumar Jaiswal – Biomaterial Processing and Products, VTT Technical Research Centre of Finland Ltd., 02044 Espoo, Finland; orcid.org/0000-0002-7797-8774; Email: aayush.jaiswal@vtt.fi

Authors

Ari Hokkanen – Microelectronics, VTT Technical Research Centre of Finland Ltd., 02044 Espoo, Finland; orcid.org/0000-0002-1200-2404

Sergei Khakalo – Integrated Computational Materials Engineering, VTT Technical Research Centre of Finland Ltd., 02044 Espoo, Finland; Department of Civil Engineering, Aalto University, 02150 Espoo, Finland

Tapio Mäkelä – Sensing Solutions, VTT Technical Research Centre of Finland Ltd., 02044 Espoo, Finland

Anniina Savolainen – Biomaterial Processing and Products, VTT Technical Research Centre of Finland Ltd., 02044 Espoo, Finland

Vinay Kumar – Biomaterial Processing and Products, VTT Technical Research Centre of Finland Ltd., 02044 Espoo, Finland

Complete contact information is available at:

<https://pubs.acs.org/doi/10.1021/acsami.3c18689>

Author Contributions

The manuscript was written through contributions of all authors. All authors have given approval to the final version of the manuscript.

Funding

The work was funded by the iBEX 2022 innovation program of VTT Technical Research Centre of Finland. The work was part of the Academy of Finland Flagship Programme under Project Nos. 318890 and 318891 (Competence Center for Materials Bioeconomy, FinnCERES) and the Academy of Finland Flagship Programme, Photonics Research and Innovation (PREIN), decision number 320168.

Notes

The authors declare no competing financial interest.

■ ACKNOWLEDGMENTS

The authors thank Altti Akujärvi for building the LabView logging system for thermocouples. Panu Lahtinen is thanked for producing the CNF material, and Timo Kaljunen is acknowledged for his input toward optimizing the CNF film preparation process.

■ REFERENCES

- (1) Santamouris, M. Cooling the Buildings – Past, Present and Future. *Energy Build.* **2016**, *128*, 617–638.
- (2) International Energy Agency (IEA). *The Future of Cooling; Paris*, 2018.
- (3) Al-Obaidi, K. M.; Ismail, M.; Rahman, A. M. A. Passive Cooling Techniques through Reflective and Radiative Roofs in Tropical Houses in Southeast Asia: A Literature Review. *Front. Archit. Res.* **2014**, *3* (3), 283–297, DOI: 10.1016/j.foar.2014.06.002.
- (4) Xiang, B.; Zhang, R.; Luo, Y.; Zhang, S.; Xu, L.; Min, H.; Tang, S.; Meng, X. 3D Porous Polymer Film with Designed Pore Architecture and Auto-Deposited SiO₂ for Highly Efficient Passive Radiative Cooling. *Nano Energy* **2021**, *81*, No. 105600.
- (5) Catalanotti, S.; Cuomo, V.; Piro, G.; Ruggi, D.; Silvestrini, V.; Troise, G. The Radiative Cooling of Selective Surfaces. *Sol. Energy* **1975**, *17* (2), 83–89.
- (6) Rephaeli, E.; Raman, A.; Fan, S. Ultrabroadband Photonic Structures to Achieve High-Performance Daytime Radiative Cooling. *Nano Lett.* **2013**, *13* (4), 1457–1461.
- (7) Li, X.; Peoples, J.; Yao, P.; Ruan, X. Ultrawhite BaSO₄ Paints and Films for Remarkable Daytime Subambient Radiative Cooling. *ACS Appl. Mater. Interfaces* **2021**, *13* (18), 21733–21739.
- (8) Mandal, J.; Yang, Y.; Yu, N.; Raman, A. P. Paints as a Scalable and Effective Radiative Cooling Technology for Buildings. *Joule* **2020**, *4* (7), 1350–1356.
- (9) Felicelli, A.; Katsamba, I.; Barrios, F.; Zhang, Y.; Guo, Z.; Peoples, J.; Chiu, G.; Ruan, X. Thin Layer Lightweight and Ultrawhite Hexagonal Boron Nitride Nanoporous Paints for Daytime Radiative Cooling. *Cell Rep. Phys. Sci.* **2022**, *3* (10), No. 101058.
- (10) Vuoriluoto, M.; Hokkanen, A.; Mäkelä, T.; Harlin, A.; Orelma, H. Optical Properties of an Organic-Inorganic Hybrid Film Made of Regenerated Cellulose Doped with Light-Scattering TiO₂ Particles. *Opt. Mater.* **2022**, *123*, No. 111882.
- (11) Zhai, Y.; Ma, Y.; David, S. N.; Zhao, D.; Lou, R.; Tan, G.; Yang, R.; Yin, X. Scalable-Manufactured Randomized Glass-Polymer Hybrid Metamaterial for Daytime Radiative Cooling. *Science* **2017**, *355* (6329), 1062–1066.
- (12) Gamage, S.; Kang, E. S. H.; Åkerlind, C.; Sardar, S.; Edberg, J.; Kariis, H.; Ederth, T.; Berggren, M.; Jonsson, M. P. Transparent Nanocellulose Metamaterial Enables Controlled Optical Diffusion and Radiative Cooling. *J. Mater. Chem. C* **2020**, *8* (34), 11687–11694.
- (13) Gentle, A. R.; Smith, G. B. Radiative Heat Pumping from the Earth Using Surface Phonon Resonant Nanoparticles. *Nano Lett.* **2010**, *10* (2), 373–379.
- (14) Gentle, A. R.; Smith, G. B. A Subambient Open Roof Surface under the Mid-Summer Sun. *Adv. Sci.* **2015**, *2* (9), No. 1500119.
- (15) Raman, A. P.; Anoma, M. A.; Zhu, L.; Rephaeli, E.; Fan, S. Passive Radiative Cooling below Ambient Air Temperature under Direct Sunlight. *Nature* **2014**, *515* (7528), 540–544.
- (16) Zhu, Y.; Luo, H.; Yang, C.; Qin, B.; Ghosh, P.; Kaur, S.; Shen, W.; Qiu, M.; Belov, P.; Li, Q. Color-Preserving Passive Radiative Cooling for an Actively Temperature-Regulated Enclosure. *Light Sci. Appl.* **2022**, *11* (1), No. 122, DOI: 10.1038/s41377-022-00810-y.
- (17) Chen, M.; Pang, D.; Chen, X.; Yan, H.; Yang, Y. Passive Daytime Radiative Cooling: Fundamentals, Material Designs, and Applications. *EcoMat* **2022**, *4* (1), No. e12153.
- (18) Fan, S.; Raman, A. Metamaterials for Radiative Sky Cooling. *Natl. Sci. Rev.* **2018**, *5* (2), 132–133.
- (19) Li, T.; Zhai, Y.; He, S.; Gan, W.; Wei, Z.; Heidarinejad, M.; Dalgo, D.; Mi, R.; Zhao, X.; Song, J.; Dai, J.; Chen, C.; Aili, A.; Vellore, A.; Martini, A.; Yang, R.; Srebric, J.; Yin, X.; Hu, L. A Radiative Cooling Structural Material. *Science* **2019**, *364* (6442), 760–763.
- (20) Huang, Y.; Zhu, C.; Yang, J.; Nie, Y.; Chen, C.; Sun, D. Recent Advances in Bacterial Cellulose. *Cellulose* **2014**, *21*, 1–30, DOI: 10.1007/s10570-013-0088-z.
- (21) Dufresne, A. Nanocellulose Processing Properties and Potential Applications. *Curr. For. Rep.* **2019**, *5* (2), 76–89.

- (22) Klemm, D.; Heublein, B.; Fink, H. P.; Bohn, A. Cellulose: Fascinating Biopolymer and Sustainable Raw Material. *Angew. Chem., Int. Ed.* **2005**, *3358–3393*, DOI: 10.1002/anie.200460587.
- (23) Moon, R. J.; Schueneman, G. T.; Simonsen, J. Overview of Cellulose Nanomaterials, Their Capabilities and Applications. *JOM* **2016**, *68* (9), 2383–2394.
- (24) Abitbol, T.; Rivkin, A.; Cao, Y.; Nevo, Y.; Abraham, E.; Ben-Shalom, T.; Lapidot, S.; Shoseyov, O. Nanocellulose, a Tiny Fiber with Huge Applications. *Curr. Opin. Biotechnol.* **2016**, *76–88*, DOI: 10.1016/j.copbio.2016.01.002.
- (25) Gamage, S.; Banerjee, D.; Alam, M. M.; Hallberg, T.; Åkerlind, C.; Sultana, A.; Shanker, R.; Berggren, M.; Crispin, X.; Kariis, H.; Zhao, D.; Jonsson, M. P. Reflective and Transparent Cellulose-Based Passive Radiative Coolers. *Cellulose* **2021**, *28* (14), 9383–9393.
- (26) Shanker, R.; Anusuyadevi, P. R.; Gamage, S.; Hallberg, T.; Kariis, H.; Banerjee, D.; Svagan, A. J.; Jonsson, M. P. Structurally Colored Cellulose Nanocrystal Films as Transreflective Radiative Coolers. *ACS Nano* **2022**, *16* (7), 10156–10162, DOI: 10.1021/acsnano.1c10959.
- (27) Chen, Y.; Dang, B.; Fu, J.; Wang, C.; Li, C.; Sun, Q.; Li, H. Cellulose-Based Hybrid Structural Material for Radiative Cooling. *Nano Lett.* **2021**, *21* (1), 397–404.
- (28) Chen, X.; He, M.; Feng, S.; Xu, Z.; Peng, H.; Shi, S.; Liu, C.; Zhou, Y. Cellulose-Based Porous Polymer Film with Auto-Deposited TiO₂ as Spectrally Selective Materials for Passive Daytime Radiative Cooling. *Opt Mater.* **2021**, *120*, No. 111431.
- (29) Lv, T.; Huang, J.; Liu, W.; Zhang, R. From Sky Back to Sky: Embedded Transparent Cellulose Membrane to Improve the Thermal Performance of Solar Module by Radiative Cooling. *Case Stud. Therm. Eng.* **2020**, *18*, No. 100596.
- (30) Li, X.; Sun, B.; Sui, C.; Nandi, A.; Fang, H.; Peng, Y.; Tan, G.; Hsu, P.-C. Integration of Daytime Radiative Cooling and Solar Heating for Year-Round Energy Saving in Buildings. *Nat. Commun.* **2020**, *11* (1), No. 6101.
- (31) Favoino, F.; Overend, M.; Jin, Q. The Optimal Thermo-Optical Properties and Energy Saving Potential of Adaptive Glazing Technologies. *Appl. Energy* **2015**, *156*, 1–15.
- (32) Dastidar, S.; Alam, M. M.; Crispin, X.; Zhao, D.; Jonsson, M. P. Janus Cellulose for Self-Adaptive Solar Heating and Evaporative Drying. *Cell Rep. Phys. Sci.* **2022**, *3* (12), No. 101196.
- (33) Fei, J.; Han, D.; Ge, J.; Wang, X.; Koh, S. W.; Gao, S.; Sun, Z.; Wan, M. P.; Ng, B. F.; Cai, L.; Li, H. Switchable Surface Coating for Bifunctional Passive Radiative Cooling and Solar Heating. *Adv. Funct. Mater.* **2022**, *32* (27), No. 2203582.
- (34) Abdellaoui, H.; Raji, M.; Chakchak, H.; el kacem Qaiss, A.; Bouhfid, R. Thermochromic Composite Materials: Synthesis, Properties and Applications. In *Polymer Nanocomposite-Based Smart Materials*; Elsevier, 2020; pp 61–78.
- (35) Jaiswal, A. K.; Hokkanen, A.; Kumar, V.; Mäkelä, T.; Harlin, A.; Orelma, H. Thermoresponsive Nanocellulose Films as an Optical Modulation Device: Proof-of-Concept. *ACS Appl. Mater. Interfaces* **2021**, *13*, 25346–25356.
- (36) Lord, S. D. *A New Software Tool for Computing Earth's Atmospheric Transmission of Near-and Far-Infrared Radiation*; Ames Research Center, 1992.
- (37) Kumar, V.; Bollström, R.; Yang, A.; Chen, Q.; Chen, G.; Salminen, P.; Bousfield, D.; Toivakka, M. Comparison of Nano- and Microfibrillated Cellulose Films. *Cellulose* **2014**, *21* (5), 3443–3456.
- (38) Jaiswal, A. K.; Kumar, V.; Jansson, E.; Huttunen, O. H.; Yamamoto, A.; Vikman, M.; Khakalo, A.; Hiltunen, J.; Behfar, M. H. Biodegradable Cellulose Nanocomposite Substrate for Recyclable Flexible Printed Electronics. *Adv. Electron. Mater.* **2023**, *9*, No. 2201094, DOI: 10.1002/aelm.202201094.
- (39) Shanmugam, K.; Doosthosseini, H.; Varanasi, S.; Garnier, G.; Batchelor, W. Flexible Spray Coating Process for Smooth Nanocellulose Film Production. *Cellulose* **2018**, *25* (3), 1725–1741.
- (40) Wang, J.; Jiu, J.; Sugahara, T.; Nagao, S.; Nogi, M.; Koga, H.; He, P.; Sukanuma, K.; Uchida, H. Highly Reliable Silver Nanowire Transparent Electrode Employing Selectively Patterned Barrier Shaped by Self-Masked Photolithography. *ACS Appl. Mater. Interfaces* **2015**, *7* (41), 23297–23304.
- (41) Penning, A. K.; Weibel, J. A. Assessing the Influence of Glass Properties on Cabin Solar Heating and Range of an Electric Vehicle Using a Comprehensive System Model. *Appl. Energy* **2023**, *339*, No. 120973.
- (42) Sun, X.; Sun, Y.; Zhou, Z.; Alam, M. A.; Bermel, P. Radiative Sky Cooling: Fundamental Physics, Materials, Structures, and Applications. *Nanophotonics* **2017**, *6* (5), 997–1015.